Received: 2 May 2021 | Revised: 7 June 2021 | Accepted: 21 June 2021

DOI: 10.1002/jcc.26717

FULL PAPER

Journal of COMPUTATIONAL CHEMISTRY WILEY

Identification of novel inhibitors of SARS-CoV-2 main protease (M^{pro}) from *Withania* sp. by molecular docking and molecular dynamics simulation

Surjeet Verma PhD[1] | **Chirag N. Patel PhD**[2] | **Muktesh Chandra PhD**[3]

[1]Department of Plant & Soil Sciences, University of Pretoria, Pretoria, South Africa

[2]Department of Botany, Bioinformatics and Climate Change Impacts Management, School of Sciences, Gujarat University, Ahmedabad, India

[3]Centre of Bioinformatics, IIDS, University of Allahabad, Prayagraj, Uttar Pradesh, India

Correspondence
Muktesh Chandra, Centre of Bioinformatics, IIDS, University of Allahabad, Prayagraj, Uttar Pradesh, India.
Email: mchandra33@gmail.com

Abstract

Since December 2019, coronavirus disease (COVID-19) has claimed the lives of millions of people across the globe. To date, no medicine is available for the responsible virus SARS-CoV-2. 3CLpro, that is, 3-chymotrypsin-like protease, the main protease (M^{pro}), has an important role in cleaving pp1a and pp1ab polyproteins. This M^{pro} serves as an important target in drug designing against COVID-19. Herein, the study includes the investigation, screening, and identification of potent leads from (*Withania* sps.), against SARS-CoV-2, using virtual screening, molecular docking, and molecular dynamics (MD) simulations. Seventy-three natural compounds from this important medicinal plant were screened. The Binding affinity was used to identify the most probable target to inhibit the M^{pro}, compounds 27-hydroxywithanolide F (W32, −11.5 kcal/mol), withanolide A (W56, −11.4 kcal/mol), and withacoagulin H (W30, −11.1 kcal/mol) showed highest binding energy. Lipinski's rule, followed by drug-likability and likeness screening, resulted in 36 molecules. Further, MD simulation of 50 ns predicted withacoagulin H possessing strong binding affinity and hydrogen-bonding interactions with the active site. The binding free energy calculation showed the most negative energy of withacoagulin H (−63.463 KJ/mol) compared to other selected compounds. The study also compared the bonding energy of already reported repurposed and newly synthesized drugs. Further, absorption, distribution, metabolism, and excretion predictions were made to found a good balance of potency. Hence the following screened compounds from *Withania* sps. could serve as the potential leads for drug development against COVID-19.

KEYWORDS
COVID-19, docking, molecular dynamics simulation, M^{pro}, pharmacokinetics, SARS-CoV-2, virtual screening, withanolides

1 | INTRODUCTION

The first case for novel severe acute respiratory syndrome coronavirus 2 (SARS-CoV-2) was reported in the live wildlife market at Hubei province of China in December 2019.[1] Since its inception, the virus has made unprecedented growth and affected the human population worldwide. Due to the increased number of cases worldwide, the World Health Organization declared it a pandemic on March 11, 2020. The novel SARS-CoV-2 infection creates a pneumonia-like condition known as COVID-19. Symptoms such as sore throat, fever, and dry cough are observed, causing complications like septic, pulmonary edema, organ failure, and Acute Respiratory Distress Syndrome.[2] In such a devastating situation development of medication are much needed.

There are four classes of coronaviruses, namely alpha, beta, gamma, and delta. SARS and Middle East respiratory syndrome (MERS) belongs to the beta category. The causative agent for COVID-19 is SARS-CoV2.[3] The virus got SARS-CoV-2, the name due to the 82% similarity of its RNA genome with SARS-CoV. The SARS-CoV-2 consists of a 30 kb long single-stranded RNA molecule with a 5′ cap and 3′ poly-A tail with positive polarity. Its virion consists of crown-shaped peplomers, with 80–160 nm in diameter.[4] The CoVs consist of four structural proteins, namely spike (S protein), envelope (E) protein, membrane (M) protein, and nucleocapsid (N) protein. The N protein participates in RNA genome packaging, and S, M, E proteins are involved in forming a viral coat.[5] The COVID-19 genome, for its replication and transcription, encodes two replicase proteins, pp1a and pp1ab.[6] The main protease (M^{pro}) releases the functional peptides from the polyproteins through extensive proteolytic processing. M^{pro} is vital for the viral life cycle as it digests the polyproteins at 11 conserved sites by autolytic cleavage by pp1a and pp1ab.[7] Moreover, the absence of homologs in humans makes it a perfect target for antiviral drug design.

As per the information, SARS-CoV-2 has a low fatality rate but spreads more efficiently than MERS and SARS-CoV, making it more difficult to stop its infection. For designing therapeutic to counter infection and devise pathology for COVID-19, it is necessary to understand how coronavirus infects the host and hijacks its machinery. The knowledge obtained can be used to design new drugs, repurpose the existing drugs, or test molecules of medicinal plants for their efficacy against the virus.

Medicinal plants serve as a vital source for many pharmacologically active structurally diverse metabolites, having their role in traditional medicinal systems and pharmaceutical industries. These metabolites, *aka* secondary metabolites, have an important functional and physiological function in plants. Metabolites differ among plants, for example, phenylpropanoids and terpenoids in *Ocimum* species, withanolides and withaferins in *Withania* species, and so on. Here, molecules from *Withania* sps were tested to get their efficacy and binding capability to the main protease of SARS-CoV-2.

In recent years, strategies such as drug repurposing have played a crucial role in speeding the drug designing against rapidly spreading infections, either be Ebola infection, Hepatitis C, Zika virus, or the SARS-CoV-2.[8–10] Repurposing investigations revealed various medications, such as lopinavir, remdesivir, lopinavir-ritonavir, hydroxychloroquine, ivermectin, and numerous other natural products and natural product-derived compounds, had good effectiveness against SARS-CoV-2.[11,12] Moreover, few other repurposed synthetic molecules have shown good inhibitory activity against SARS-CoV-2 M^{pro} *in-vitro*.[6,13] Several molecules isolated from various plants such as *Glycyrrhiza glabra*, *Asparagus rasemosus*, *Ocimum basilicum*, *Ocimum sanctum*, *Clonorchis sinensis*, and *Withania somnifera*, and so forth, also exhibit antiviral properties.[14–16] Recently, few phyto-molecules including oolonghomobisflavan-A, theasinensin-D, theaflavin-3-*O*-gallate, glycyrrhizic acid, asparoside-C, D, and F have been identified as potential inhibitors of SARS-CoV-2 M^{pro} and spike protein in several *in-silico* studies.[17–19] The glycyrrhizic acid, its derivatives, and other triterpenes have shown great inhibition potential against SARS-CoV replication and cytopathic effect *in-vitro*. Due to the 82% of RNA genome similarity between SARS-CoV and SARS-CoV-2, Verma et al.[11] have hypothesized that these compounds or similar compounds may potentially inhibit SARS-CoV-2 viral replication and infection as well. Furthermore, few similar steroidal glycosides such as abiraterone acetate, ouabain, digoxin, and digitoxin have shown promising *in-vitro* inhibitory activity against SARS-CoV-2.[12]

Following this hypothesis having the close structural similarity to these compounds, 73 withanolides isolated from five *Withania* species were selected from the literature and screened virtually. Further, the rule of five analyses reduced the list of molecules. *In-silico* studies, including molecular docking simulation, were done to screen the potential inhibitors for M^{pro} of SARS-CoV-2. Absorption, distribution, metabolism, and excretion (ADME) prediction provided the bioavailability score (ABS) and permeability of molecules which act as an essential factor for drug designing. Furthermore, we envisage that *in-vitro* and *in-vivo* studies should be conducted for better inhibitory potential on these selected molecules, serving as a template for drug design for M^{pro} from SARS-CoV-2.

2 | MATERIALS AND METHODS

2.1 | Compilation of dataset

The three-dimensional structure of SARS-CoV-2 M^{pro}, PDB ID 6Y2F, with a resolution of 1.95, was retrieved from the protein data bank.[3] The structure of reference compounds (**RC1-5**) and 73 *Withania* compounds (**W1-73**) were collected from the literature.[6,11,20] The local database of names and structures of all the compounds (Table S1) was created by drawing their structure through ChemDraw ultra12 and saved in SDF format. These 2D formats of molecules were transformed to the 3D coordinates and optimized using the GUI version of Openbabel2.3.2.[21]

2.2 | Molecule preparation and grid generation

The crystal structure was prepared for binding analysis using Autodock Tools (ADT).[22] Protein preparation included adding charges (Gasteiger charges), polar hydrogens, and optimizing the rotatable bonds. Prepared protein was thus saved in pdbqt format for further analysis. The idea of a binding site was obtained from already available information the coordinates around the centre atom of the active site considered for the generation of the grid box. ADT received the information of the grid box based on the above information. The grid box for PDB ID 6Y2F considered was with coordinates as 10.601, −0.613, and 21.174 for *x*, *y*, and *z*-axis, respectively. The size of the grid box was manually adjusted and set as 20.180 × 20.180 × 20.180. The configuration file was created using the receptor, ligand, and grid parameters information before the final execution of the molecular docking. In the virtual screening process, already reported drug

molecules, lopinavir, and RC1-4 were used as control molecules throughout the study.

All the biomolecules and the control molecules were prepared using ADT by adding polar hydrogen and gasteiger charges. After adjusting the rotatable bonds and torsion angle, each of the molecules was saved in pdbqt format. The molecular docking output files were analyzed based on ligand and protein binding energy and interactions profile. The protein-ligand interaction profile was utilized to evaluate the interactions.

2.3 | ADME risk and rule of five based screening

Lipinski's rule of five was considered the primary factor for screening the molecules.[23] After screening, the molecules were subjected to ADME risk assessment software to ascertain their risk for drugability. Physiochemical properties were evaluated to understand the oral activity of molecules through Lipinski's rules.

2.4 | Pharmacokinetics compliance evaluation

Most drugs fail in the discovery process in reaching clinical trials, which happens due to poor pharmacokinetics (PK). The PK properties were calculated for drug testing toward ADME.[24] The study included physiochemical properties estimation (such as molecular weight [MW], topological polar surface area [TPSA]), lipophilicity (indicated by log *P*, and consensus log *P*), water solubility (indicated by log *S*, on a scale of −10 [insoluble] to 0 [highly soluble]), pharmacokinetics (gastrointestinal [GI] absorption, BBB permeant for blood–brain barrier, log *Kp* for skin permeability), drug-likeness (included Lipinski, Ghose, Egan, and bioavailability), and so forth. The process of excreting the drug from the body depends on log *P* and MW.

2.5 | Molecular dynamics simulation studies

The Desmond (Schrodinger Release 2019-3) package was used for molecular dynamic (MD) simulations[25] with the top three *Withania* compounds of the SARS-CoV-2 M^{pro} target. The experiment included simulations for 50 ns followed by plotting various matrices to check the stability of structures. The protein preparation wizard at the Schrodinger interface was used to create protein starting structures. For this bond orders assignments, the addition of hydrogens, and filling of missing amino acid chain and loops, and hydrogen bond assignment optimization. System Builder module applied to build the periodic simulation box and single point charge water model used for salvation, with Optimized Potentials for Liquid Simulations (OPLS) all-atom force field. The system was minimized using the steepest descent technique for 1000 iterations. After equilibration, the unrestrained production phase ran under NPT (number of atoms, pressure, and temperature were kept constant) ensemble for 50 ns at 300 K temperature and 1.01325 bar pressure. Nosé–Hoover thermostat (relaxation time = 1 ps) and the isotropic Martyna–Tobias–Klein barostat (relaxation time = 2 ps) were applied. Short-range interactions (cutoff = 9 Å) and long-range Coulombic interactions were evaluated using the smooth particle mesh Ewald (PME) method with the RESPA integrator. The conformations captured in the simulation trajectories were exported at every 5 ps. After completing simulations, the system's stability was assessed using root mean square deviation (RMSD), root mean square fluctuations (RMSF), Hydrogen bond analysis, the radius of gyration (rGyr), and the histogram for torsional bonds.

2.6 | Binding free energy calculation (MM/GBSA)

To ascertain the binding free energy of protein-ligand complex calculations are made based on Molecular mechanics generalized Born surface area (MM/GBSA). A total 50 ns trajectory was submitted to the prime module of Schrödinger to perform MM/GBSA calculations.[26] Estimations of free energy are based on the following equation

$$\text{MM/GBSA } \Delta G_{\text{bind}} = \Delta G_{\text{complex}} - \Delta G_{\text{receptor}} - \Delta G_{\text{ligand}},$$

where, ΔG is free energy for the respective complex, receptor, and ligand.

3 | RESULTS AND DISCUSSION

Literature survey helped in identifying the 73 phytochemicals isolated from *Withania somnifera (L.) Dunal*, *Withania coagulans (Stocks) Dunal*, *Withania adpressa Coss*, *Withania aristata* (Aiton) Pauquy, *Withania frutescens* (L.) Pauquy, and *Withania obtusifolia Täckh*. Few repurposed drugs/synthetic compounds, including ebselen (**RC1**), tideglusib (**RC2**), and two feline drugs, GC373 (**RC3**), and GC376 (**RC4**), have shown significant inhibitory potential against SARS-CoV-2 M^{pro}.[6,13] These compounds and lopinavir (**RC5**, an HIV protease inhibitor) were selected as reference compounds in this study (Figure S1).

3.1 | Molecular docking studies

In the current scenario, virtual screening of phytochemicals plays an important part in the drug discovery process. Virtual screening performed based on pharmaco-informatics approach utilizing *in-silico* tools plays a pivotal role in discovering drug against the pathogen.[27] M^{pro} of SARS-CoV-2 is a dimeric cysteine protease, with two promoters oriented at right angles to each other.[28] SARS M^{pro} active site is similar to that of human CoV (HCoV) and porcine transmissible gastroenteritis virus, consisting of a Cys-His dyad with positional variations.[28] Coronavirus utilizes chymotrypsin-like protease and papain protease to cleave long polyprotein precursors into individual functional Nsps, essential for virus life.[5] Hence, M^{pro} becomes the main target for anti-coronavirus drug development. A set of 73 molecules

were docked to the binding site of M^{pro}, and prioritization was made based on interaction energy scores. Molecule W48 (−13.0 kcal/mol), W32 (−11.5 kcal/mol), W56 (−11.4 kcal/mol), W30 (−11.1 kcal/mol), W60 (−11.0 kcal/mol), W52 (−10.9 kcal/mol), W34 (−10.8 kcal/mol), and W55 (−10.6 kcal/mol) binding affinity (Table 1 and Table S1) were more than that of RC1 (−5.8 kcal/mol), RC2 (−6.9 kcal/mol), RC3 (−7.7 kcal/mol), RC4 (−8.3 kcal/mol), and RC5 (−7.1 kcal/mol). The other molecules also showed good binding scores as defined (Table S1). The discovery studio visualizer examined the interacting residues between the active site and selected molecules. Re-docking of the initial inhibitor was conducted with SARS-CoV-2 M^{pro} and found 0.00 Å RMSD between the docked pose and crystal structure available RCSB database.

Further, PDB ID: 7BRR and PDB ID: 7BQY, crystal structures of M^{pro} checked for binding energy with the screened molecules' significant activity with the same molecules was observed. Autodock-vina and Autodock are robust tools utilizing the Lamarckian algorithm to fit the molecule into an active site.[22,29] The binding score obtained by these tools acts as deciding factor for screening the large set of molecules and makes a positive impact in the process of drug discovery.[10,19,30]

3.2 | Screening through the rule of five

Drug discovery requires passing out drug candidate molecules in subsequent preclinical, clinical, and further commercial phases of drug development. The development of automated and improved *in-silico* methods had increased the ability to dissect the fundamentals of ADME/PK. Undesirable and dispossessed pharmacokinetic properties become the primary reason for the compound to phase out from the process of drug discovery. Lipinski's rule was used to filter the compounds and assess the chemical properties related to oral bioavailability. Out of 73 natural biomolecules from *Withania*, only 36 could make it through the rule of five with zero violations (Table 2). These 36 compounds were further evaluated for pharmacokinetics compliance, including ADME. To avoid failure at later stages of drug development, compliance with pharmacokinetic parameters are of utmost importance. Despite having a high binding affinity, compounds W48, W51, W52, W54, W60, and W61 did not pass the rule of five and hence were not included in further testing.

TABLE 1 Inhibition constant (*Ki*) *in-silico* obtained by molecular docking for the reference and top nine compounds

S. no.	Ligands	Binding affinity[a]	Ki (Molar)[b]
1.	RC1	−5.8	5.41E-05
2.	RC2	−6.9	8.39E-06
3.	RC3	−7.7	2.16E-06
4.	RC4	−8.3	7.83E-07
5.	RC5	−7.1	5.98E-06
6.	W32	−11.5	3.46E-09
7.	W56	−11.4	4.10E-09
8.	W30	−11.1	6.82E-09
9.	W34	−10.8	1.13E-08
10.	W55	−10.6	1.59E-08
11.	W62	−10.4	2.23E-08
12.	W33	−10.0	4.39E-08
13.	W36	−10.0	4.39E-08
14.	W39	−9.9	5.21E-08

[a]Docking scores (kcal/mol) corresponds to the virtual screening scores as provided through autodock tools.
[b]*Ki* values are *in-silico* values in molar calculated using the anaconda python script.

3.3 | Binding site analysis of selected molecules

In-silico inhibition constant (*Ki*) expresses the inhibitor concentration required to inhibit the chemical reaction 50% at a specific substrate concentration.[31] *Ki* value of the top nine molecules and reference compounds were predicted as per docking score (Table 1). Molecular docking provides a stable complex comprising confirmation with the best-fit ligand in the substrate-binding pocket. The bonding pattern was established to substantiate the docking results. It was found that molecules formed the bonding with Cys-His dyad, either be through hydrogen bond (H-bond), van der Waals (VdW), and Pi-alkyl interactions, and so forth. After exploring the interactions, W32 manifests three H-bond with Gln^{192} and Thr^{190}, two Pi-Alkyl bonding with His^{41} and Cys^{145}, and VdW with Thr^{25}, Met^{49}, Asn^{142}, Gly^{143}, His^{164}, Met^{165}, Glu^{166}, Pro^{168}, Arg^{188}, and Gln^{189}. In W56 residue, Gly^{143} formed H-bond and residues His^{41}, Met^{49}, and Met^{165} formed Pi-alkyl interactions and VdW with residues Thr^{25}, Thr^{26}, Leu^{27}, Asn^{142}, Cys^{145}, His^{164}, Glu^{166}, Asp^{187}, Arg^{188}, Gln^{189}, Thr^{190}, and Gln^{192}. W30 manifests four H-bond with Gly^{143}, Arg^{188}, Thr^{190}, and Gln^{192}, while two Pi-alkyl bonds are established with His^{41} and Cys^{145} and VdW Thr^{25}, Thr^{26}, Leu^{27}, Met^{49}, Asn^{142}, Ser^{144}, His^{164}, Met^{165}, Gln^{166}, and Gln^{189}. W34 forms four H-bond with residues Thr^{190}, Gln^{192}, and Gly^{143}, two Pi-Alkyl bonds with His^{41} and Cys^{145} and VdW with residues Thr^{25}, Thr^{26}, Leu^{27}, Met^{49}, Asn^{142}, Ser^{144}, His^{164}, Met^{165}, Arg^{188}, and Gln^{189}. Likewise W55 forms four H-bond with Asn^{142}, Ser^{144}, Cys^{145}, and His^{163} and VdW with residues Thr^{24}, Thr^{25}, Thr^{26}, Leu^{27}, His^{41}, Cys^{44}, Thr^{45}, Phe^{140}, Gly^{143}, Glu^{166}, and His^{172} (Figure 1 (A,B,D,G,H) and Table 3). Similarly, H-bond, Pi-alkyl bonds, and VdW by W62, W33, W36, and W39 (Figure 1(C,E,I) and Table 3). The *in-vitro* tested molecules were also analyzed for binding residues, and they also showed binding with the HisCys dyad. In RC5, the three H-bond formed with Gly^{143}, Ser^{144}, and Glu^{166}, Pi-alkyl bond with Met^{49} and $Met^{165.}$ and VdW with Thr^{25}, Leu^{27}, Leu^{141}, His^{164}, Leu^{167}, Pro^{168}, Asp^{187}, Arg^{188}, Gln^{189}, Thr^{190}, and Gln^{192}. Similar chemical molecule RC1 showed three H-bonds Gly^{143}, Ser^{144}, and Cys^{145}, one Pi-sigma (Asn^{142}), and one Pi-Alkyl bond (Cys^{145}). RC2 manifested one H-bond with Glu^{166} and one three Pi-Alkyl interactions with His^{41}, Met^{165}, and Cys^{145}, RC3 interaction through H-bonds with residues Phe^{140} and Glu^{166} and His^{41}, and Cys^{145} forms Pi-Alkyl interactions.

TABLE 2 Compliance of screened molecules with Lipinski's rule

Code	Compound name	MW (20 ≤ X ≤ 500) g/mol	TPSA (20 ≤ X ≤ 130) Å^2	H-bond donors (≥4)	H-bond acceptors (≥7)	Rotatable bonds (≤9)	Rule of five violation
W1	(17*S*,20*S*,22*R*)-14α,15α,17β,20β-Tetrahydroxy-1-oxowitha-2,5,24-trienolide	486.6	124.29	4	7	2	0
W2	Withanolide F	470.6	104.06	3	6	2	0
W3	Withanolide J	470.6	104.06	3	6	2	0
W6	Witharistatin	468.58	96.36	2	6	3	0
W9	4β-Hydroxy-1-oxo-5β,6β-epoxywitha-2,24-dienolide	454.6	76.13	1	5	2	0
W10	4β-Hydroxy-1-oxo-5β,6β-epoxy-22*R*-witha-2,14,24-trienolide	452.58	76.13	1	5	2	0
W14	(20*S*,22*R*)-27-Hydroxy-1,4-dioxo-witha-2,5,16,24-tetraenolide	450.57	80.67	1	5	3	0
W15	(4*S*,22*R*)-4,16,27-Trihydroxy-1-oxo-witha-2,5,17(20),24-tetraenolide	468.58	104.06	3	6	2	0
W16	(4*S*,20*S*,22*R*)-4,27-Dihydroxy-1-oxo-witha-2,5,16,24-tetraenolide	452.58	83.83	2	5	3	0
W19	4β,27-Dihydroxy-1-oxo-witha-2,5,24-trienolide	454.6	83.83	2	5	3	0
W23	Obtusifonolide	496.64	89.9	1	6	5	0
W26	Isowithanone	470.6	96.36	2	6	2	0
W29	Withacoagulin G	470.6	104.06	3	6	3	0
W30	Withacoagulin H	468.58	104.06	3	6	3	0
W31	Withacoagulin I	470.6	104.06	3	6	2	0
W32	Ajugin E	486.6	124.29	4	7	3	0
W33	(20*R*, 22R-14α, 20α)-Dihydroxy1-oxowitha-2,5,16,24 tetraenolide	452.58	83.83	2	5	2	0
W34	Withacoagulin	452.58	83.83	2	5	3	0
W35	Withanolide H	470.6	104.06	3	6	3	0
W36	Withanolide G	454.6	83.83	2	5	2	0
W37	Coagulin C	452.58	72.83	1	5	1	0
W38	17β-Hydroxywithanolide K	470.6	104.06	3	6	2	0
W39	Deglucosylcoagulin L	488.61	124.29	4	7	2	0
W41	Withanolide L	452.58	83.83	2	5	2	0
W42	Withacoagulin A	452.58	83.83	2	5	2	0
W43	Withacoagulin C	486.6	124.29	4	7	2	0
W44	Withacoagulin D	486.6	124.29	4	7	3	0
W45	Withacoagulin E	454.6	83.83	2	5	2	0
W47	5β,6β,14α,15α-Diepoxy-4β,27-dihydroxy-1-oxowitha-2,24-dienolide	484.58	108.89	2	7	3	0
W55	(20*S*,22*R*)-3α,6α-Epoxy-4β,5β,27-trihydroxy-1-oxowitha-24-enolide	488.61	113.29	3	7	3	0
W56	Withanolide A	470.6	96.36	2	6	2	0
W57	(20*S*,22*R*)-4β,5β,6α,27-Tetrahydroxy-1-oxowitha-2,24-dienolide	488.61	124.29	4	7	3	0
W62	Viscosalactone B	488.61	116.59	3	7	3	0
W66	2,3-Dihydrowithaferin A	472.61	96.36	2	6	3	0
W68	17α-Hydroxywithaferin A	486.6	116.59	3	7	3	0
W73	Withaferin A	470.6	96.36	2	6	3	0

Abbreviations: H-bond, hydrogen bond; MW, molecular weight; TPSA, topological polar surface area.

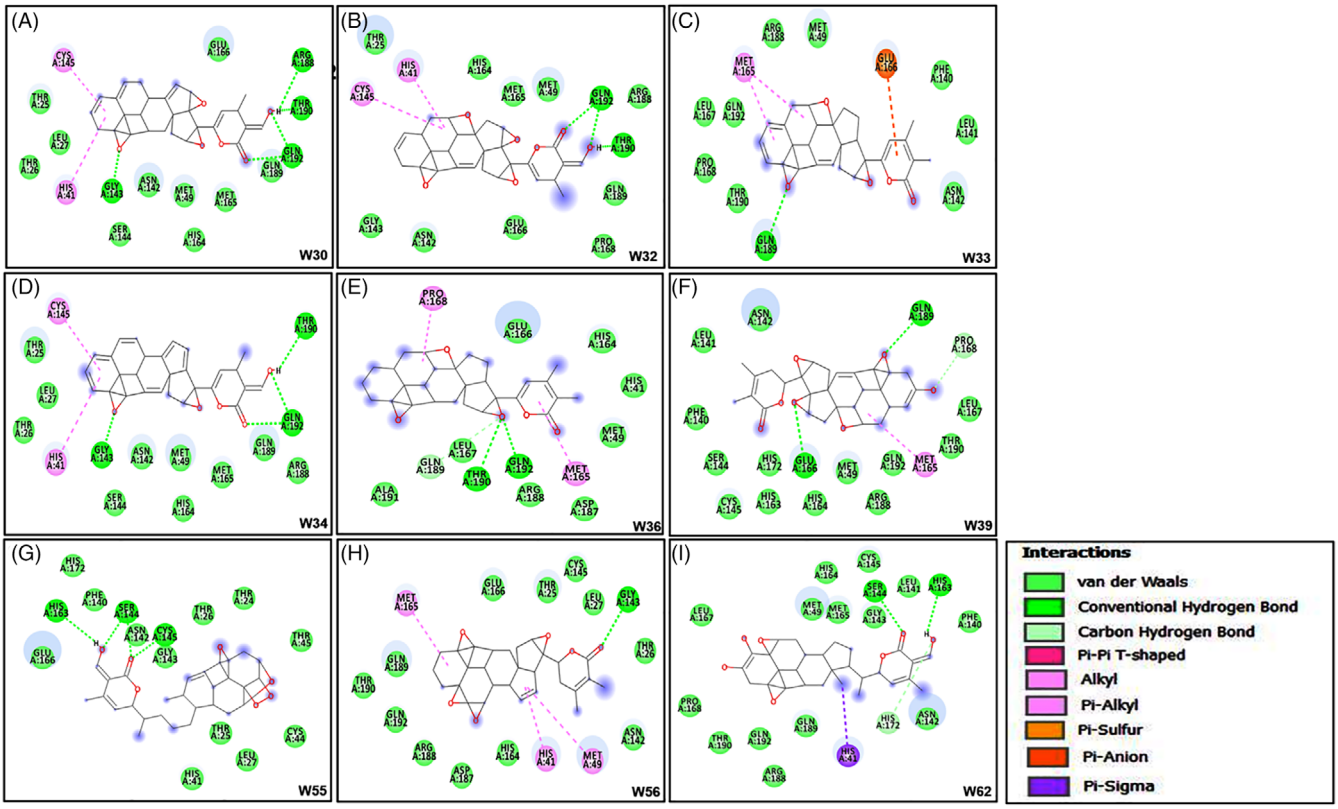

FIGURE 1 Interacting residues of top nine phytomolecules (2D format) with SARS-CoV-2 M^{pro} (i) withacoagulin H (W30), (ii) ajugin E (W32), (iii) (20*R*, 22R-14α, 20α)-dihydroxy1-oxowitha-2,5,16,24 tetraenolide (W33), (iv) withacoagulin (W34), (v) withanolide G (W36), (vi) deglucosylcoagulin L (W39), (vii) (20*S*,22*R*)-3α,6α-epoxy-4β,5β,27-trihydroxy-1-oxowitha-24-enolide (W55), (viii) withanolide A (W56), (ix) viscosalactone B (W62)

Likewise, in RC4, six H-bonds formed with His^{41}, Gly^{143}, Ser^{144}, Cys^{145}, and His^{164}, one Pi-alkyl bond formed with His^{41} and VdW interactions were also manifested (Figure 2 and Table 3). Hydrogen bonds are intermolecular interactions, play an important role in determining molecular aggregations and conformations. Their presence becomes an important factor in governing the dynamics and functions.[32] Binding interactions such as H-bond, carbon-hydrogen bonds, π-alkyl, alkyl, Pi-sigma, Van der Waals, and so forth interactions play an important role in the binding of the molecule to the substrate.

3.4 | Assessment of drug-likeness

Further, drug-like physicochemical properties were calculated by Lipinski's rule of five for the candidate compounds. Drug likeness is an essential consideration in the early phases of drug discovery for compound selection with desired bioavailability.[33] Approaches such as a quantitative estimate of drug-likeness,[32] oral PhysChem score,[33] ABS,[34] or Gaussian scoring function[35] include physiochemical parameters into the drug-likeness score, assisting in compound screening. Physiochemical properties such as permeability, lipophilicity, solubility, affinity, and metabolic stability were also assessed. Screened compounds ABS was 0.55, which signifies that the compounds passed Lipinski's rule of five.[23] ADME and molecular PK were also taken into consideration. Such as solubility with water, absorption by the intestine, hepatotoxicity, plasma protein binding, GI absorption, blood–brain penetration (BBB), and interaction with cytochrome P450 (CYP). Rules define, though, cannot predict the pharmacological activity of compounds. Yet, these rules in a well-defined stepwise manner play a crucial role in determining the significant lead molecules for protein specificity and biological activity. To adjudicate the significance of compounds, MW is considered the essential factor, that is, MW of the compound should be between 150 and 500 g/mol (Table 2). Lipophilicity is signified as the coefficient between *n*-octanol and water (log $P_{o/w}$), that is, the ratio of solubility of the compound in octanol compared to its solubility in an aqueous medium. MW in collaboration with log *P* defined as an important factor for permeability. Similarly, water solubility determined by log *S* value which did not exceeded six for compound to be soluble. log *S* along with determinants such as MW, number of rotatable bonds, fraction of aromatic heavy atoms and log *P*, defines the compounds are soluble in aqueous medium (Table 4).

The candidate compounds have high bioavailability because they do not violate Lipinski's rule of five, that is, their molecular mass is below 500 Da, they possess high lipophilicity (log $P < 5$), hydrogen donors (<5), hydrogen acceptors (<10), and, their molar refractivity lie

TABLE 3 Binding residues of top nine compounds and reference compounds, obtained through molecular docking

S. no.	Compounds	Interacting residues[a]
1.	RC1	Thr25, Thr26, Leu27, **His41**, Phe140, Leu141, **Asn142**, **Gly143**, Ser144, **Cys145**, Glu166
2.	RC2	**His41**, **Met49**, Phe140, Leu141, **Asn142**, **Gly143**, Ser144, **Cys145**, His163, **His164**, **Met165**, Glu166, Asp187, **Arg188**, **Gln189**, **Gln192**
3.	RC3	Thr25, **His41**, **Met49**, Phe140, Leu141, **Asn142**, **Gly143**, Ser144, **Cys145**, His163, **His164**, **Met165**, Glu166, His172, **Arg188**, **Gln189**, Thr190, **Gln192**
4.	RC4	Thr25, Leu27, **His41**, **Met49**, Phe140, Leu141, **Asn142**, **Gly143**, Ser144, **Cys145**, His163, **His164**, **Met165**, Glu166, Leu167, Pro168, Asp187, **Arg188**, **Gln189**, **Gln192**
5.	RC5	Thr25, Leu27, **His41**, **Met49**, Leu141, **Asn142**, **Gly143**, Ser144, **Cys145**, **His164**, **Met165**, Glu166, Leu167, Pro168, Asp187, **Arg188**, **Gln189**, Thr190, **Gln192**
6.	W32	Thr25, **His41**, **Met49**, **Asn142**, **Gly143**, **Cys145**, **His164**, **Met165**, Glu166, Pro168, **Arg188**, **Gln189**, Thr190, **Gln192**
7.	W56	Thr25, Thr26, Leu27, **His41**, **Met49**, **Asn142**, **Gly143**, **Cys145**, **His164**, **Met165**, Glu166, Asp187, **Arg188**, **Gln189**, Thr190, **Gln192**
8.	W30	Thr25, Thr26, Leu27, **His41**, **Met49**, **Asn142**, **Gly143**, Ser144, **Cys145**, **His164**, **Met165**, Gln166, **Arg188**, **Gln189**, Thr190, **Gln192**
9.	W34	Thr25, Thr26, Leu27, **His41**, **Met49**, **Asn142**, **Gly143**, Ser144, **Cys145**, **His164**, **Met165**, **Arg188**, **Gln189**, Thr190, **Gln192**
10.	W55	Thr24, Thr25, Thr26, Leu27, **His41**, Cys44, Thr45, Phe140, **Asn142**, **Gly143**, Ser144, **Cys145**, His163, Glu166, His172
11.	W62	**His41**, **Met49**, Phe140, Leu141, **Asn142**, **Gly143**, Ser144, **Cys145**, His163, **His164**, **Met165**, Leu167, Pro168, His172, **Arg188**, **Gln189**, Thr190, **Gln192**
12.	W33	**Met49**, Phe140, Leu141, **Asn142**, **Met165**, Glu166, Leu167, Pro168, **Arg188**, **Gln189**, Thr190, **Gln192**
13.	W36	**His41**, **Met49**, **His164**, **Met165**, Glu166, Leu167, Pro168, Asp187, **Arg188**, **Gln189**, Thr190, Ala191, **Gln192**
14.	W39	**Met49**, Phe140, Leu141, **Asn142**, Ser144, **Cys145**, His163, **His164**, **Met165**, Glu166, Leu167, Pro168, His172, **Arg188**, **Gln189**, Thr190, **Gln192**

Note: Most common residues are highlighted in bold.
[a]Interacting residues shown are within the 4 Å vicinity of ligands.

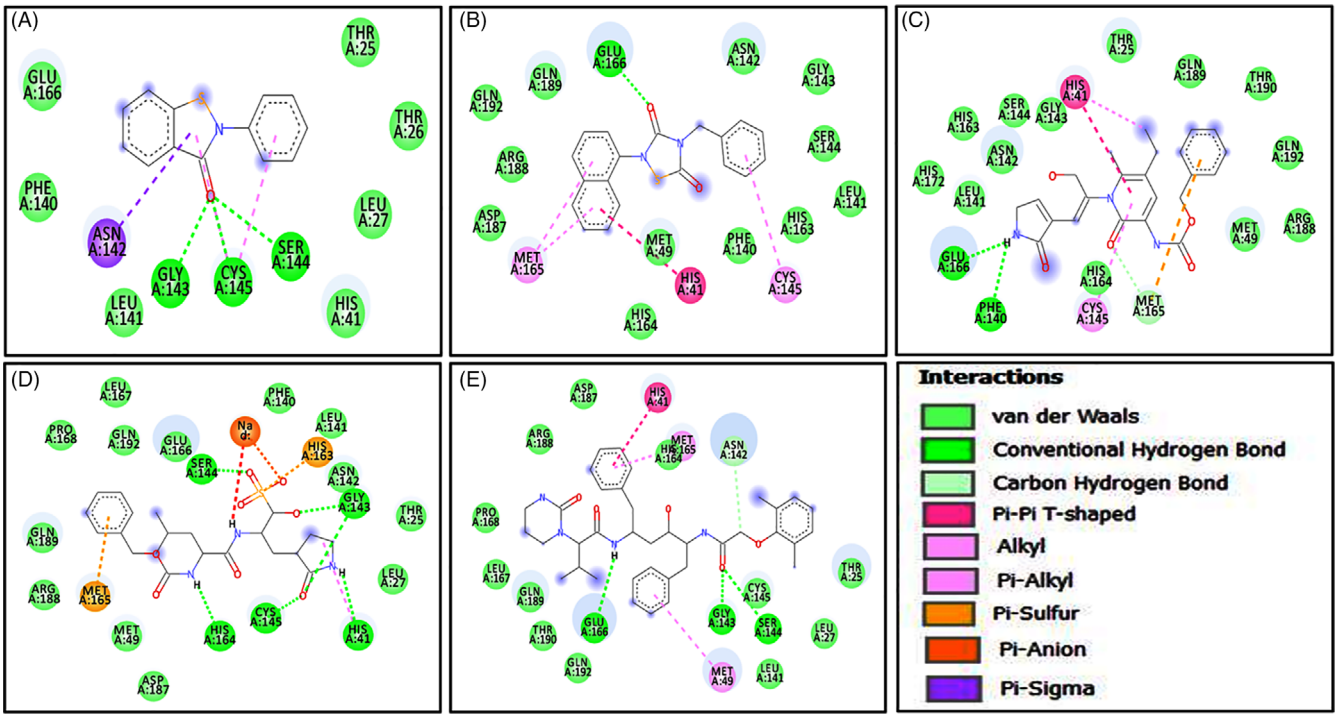

FIGURE 2 Interacting residues of reference compounds (2D format) with SARS-CoV-2 M^{pro} (i) ebselen (RC1), (ii) tideglusib (RC2), (iii) GC373 (RC3), (iv) GC376 (RC4), (v) lopinavir (RC5)

Compounds	log *S* (solubility)	log *Kp*	log *P*	CYP1A2	BBB permeant
W33	−4.33	−7.02	3.65	No	No
W36	−4.71	−6.61	3.9	No	No
W56	−4.67	−6.86	3.39	No	No
W32	−3.74	−8.05	2.67	No	No
W30	−3.94	−7.59	2.96	No	No
W39	−3.51	−8.41	2.41	No	No
W34	−4.62	−6.61	3.77	No	No
W55	−4.47	−7.26	2.73	No	No
W62	−4.47	−7.26	2.8	No	No

Note: All the values predicted are by Swiss-ADME analysis server.

TABLE 4 Compliance of screened molecules with standard ranges of ADME and drug-likeness

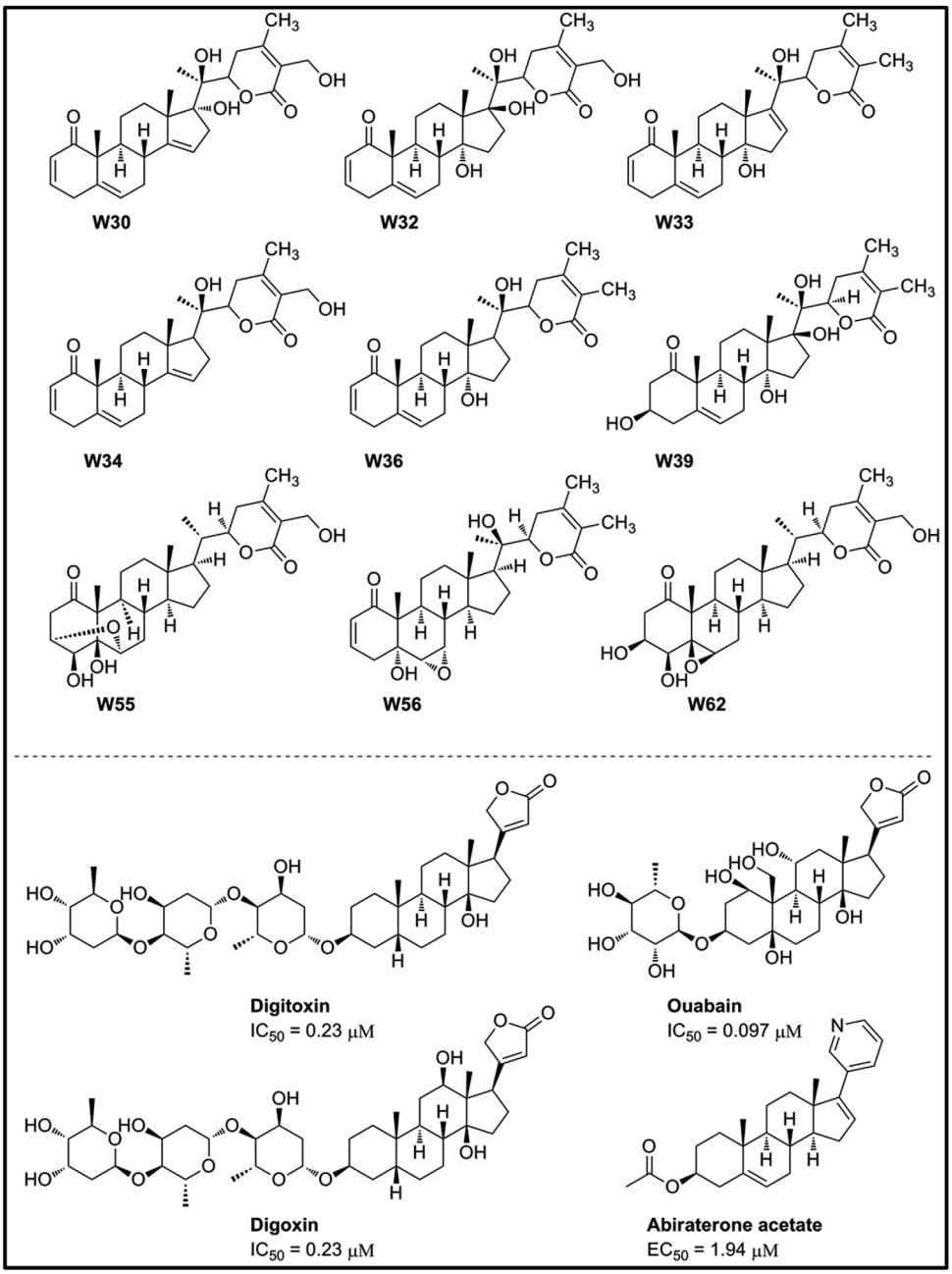

FIGURE 3 Chemical structure top nine screened phytomolecules namely withacoagulin H (W30), ajugin E (W32), (20*R*, 22R-14α, 20α)-dihydroxy1-oxowitha-2,5,16,24 tetraenolide (W33), withacoagulin (W34), withanolide G (W36), deglucosylcoagulin L (W39), (20*S*,22*R*)-3α,6α-epoxy-4β,5β,27-trihydroxy-1-oxowitha-24-enolide (W55), withanolide A (W56), viscosalactone B (W62) and few similar molecules with in-vitro anti-SARS-CoV-2 activity (digitoxin, ouabain, digoxin, and abiraterone acetate)

in between 40 and 130. Moreover, when we calculated the TPSA for passive molecular transport through membranes, the result showed their values were <130 Å^2. Its a general observation that compounds with TPSA>140 Å^2 have low oral bioavailability. Furthermore, GI absorption values, BBB permeation calculated to see whether the compounds show active efflux through biological membranes, that is, through the GI wall to lumen or from the brain. Additionally, CYP interactions were calculated to understand drug elimination through biotransformation. CYP interaction plays an important step in clearing a drug or its metabolite from the body leading to low/high toxicity. The values of our probable compounds were within the range of standard drugs (Table 4).

As a result, the top nine molecules identified in this study that have the potential to inhibit SARS-CoV-2 M^{pro} include withacoagulin H (W30), 27-hydroxywithanolide F or ajugin E (W32), (20R, 22R-14, 20α)-dihydroxy1-oxowitha-2,5,16,24 tetraenolide (W33), withacoagulin (W34), withanolide G (W36), deglucosylcoagulin L (W39), (20S,22R)-3α,6α-epoxy-4β,5β,27-trihydroxy-1-oxowitha-24-enolide (W55), withanolide A (W56), viscosalactone B (W62) (Figure 3). As evident from Table 2, all of these compounds showed better binding affinity to SARS-CoV-2 M^{pro} than the reference compounds (RC1-5). Hence, these compounds could exhibit more potent inhibitory activity than the RC1-5 in *in-vitro* assessments. The *in-vitro* half-maximum inhibitory concentration (IC_{50}) values for the reference compounds ebselen (RC1), tideglusib (RC2), GC373 (RC3), and GC376 (RC4) are quite low, 0.67, 1.55, 0.40, and 0.19 μM, respectively.[6,13] Few other similar compounds like digitoxin, digoxin, and ouabain have been reported to have *in-vitro* anti-SARS-CoV-2 activity with significantly lower IC_{50} values of 0.23, 0.19, and 0.097 μM, respectively. Another similar compound, abiraterone acetate, has been reported to exhibit anti-SARS-CoV-2 activity with 50% maximal effective concentrations (EC_{50}) of 1.94 μM.[12]

Compounds **W30-36** have been isolated from *W. coagulans* while **W39** is a semisynthetic derivative of coagulin L (**W4**), Coagulin L has been isolated from *W. adpressa* as well as *W. coagulans*, and compounds **W55-62** isolated from *W. somnifera*. Hence, from these results, it can be concluded that out of five species, *W. adpressa*, *W. coagulans*, and *W. somnifera* may have great potential to inhibit SARS-CoV-2 (COVID-19). However, the *in-vitro* assessment is still to be done for the confirmation of the same. Apart from this, these plant species have been well known for their immune-boosting potential,[11] which is further advantageous in COVID-19 treatment. Compounds **W30-36** have also been reported to show significant inhibition of nitric oxide (NO) production, tumor necrosis factor-α, and induced nuclear factor-kappa B (NF-κB). The infection with SARS-CoV-2 also activates transcription factors such as NF-κβ. Hence, these compounds might also help reduce such complications. Compound **W39** exhibited significant inhibition of the postprandial rise in hyperglycemia and post-sucrose load in normoglycemic and streptozotocin-induced diabetic rats. Since COVID-19 has been well known for its secondary complications with diabetic patients, **W39** and *W. coagulans* will be further advantageous for COVID-19 treatment in diabetic patients. Compounds **W55** and **56** have also been reported for their significant neurite outgrowth activity. Compound **W62** has been reported for its selective inhibitory activity against cyclooxygenase-2 (COX-2) enzyme and lipid peroxidation. Patients infected with SARS-CoV-2 have several inflammatory complications as well. Hence, these compounds and respective plant species might

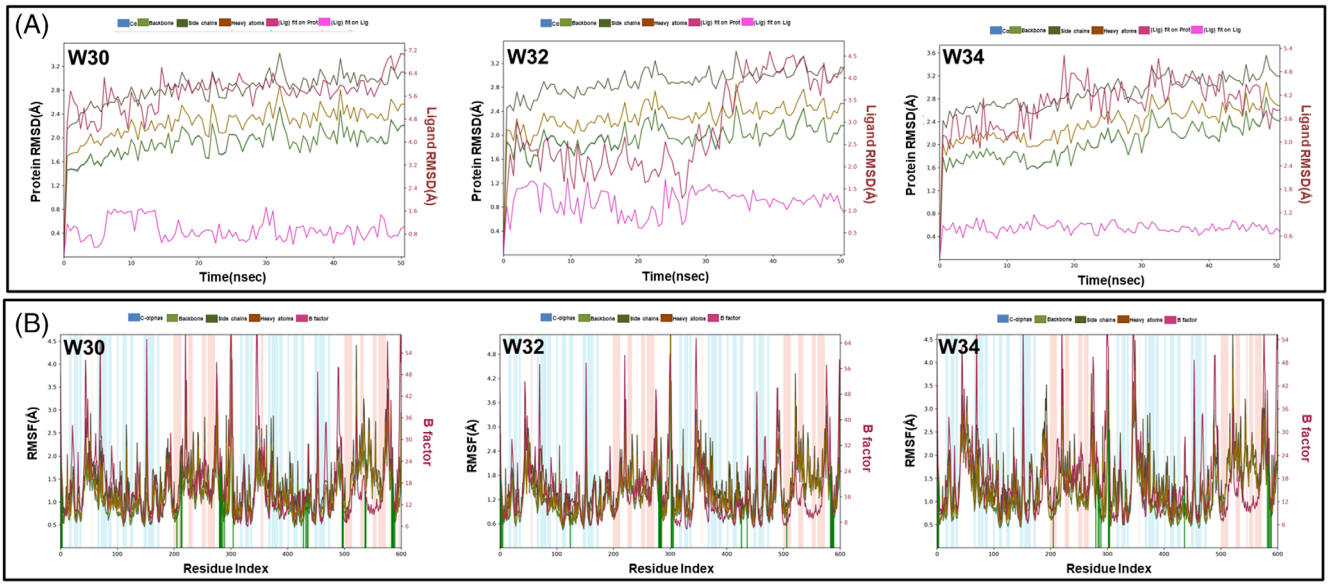

FIGURE 4 (A) Root mean square deviation (RMSD) plot of top three compounds as a function of time. RMSD evolution of protein shown on left Y-axis, Ligand RMSD shown on right Y-axis. Key for the respective color code is provided above of individual figure frame. (B) Root mean square fluctuations (RMSF) plot for top three compounds. B-factor shown on right Y-axis, and RMSF on left Y-axis. Alpha-helical and beta-strand regions are highlighted in red and blue backgrounds respectively. Protein residues that interact with the ligand are marked with green-colored vertical bars. withacoagulin H (W30), ajugin E (W32), and withacoagulin (W34)

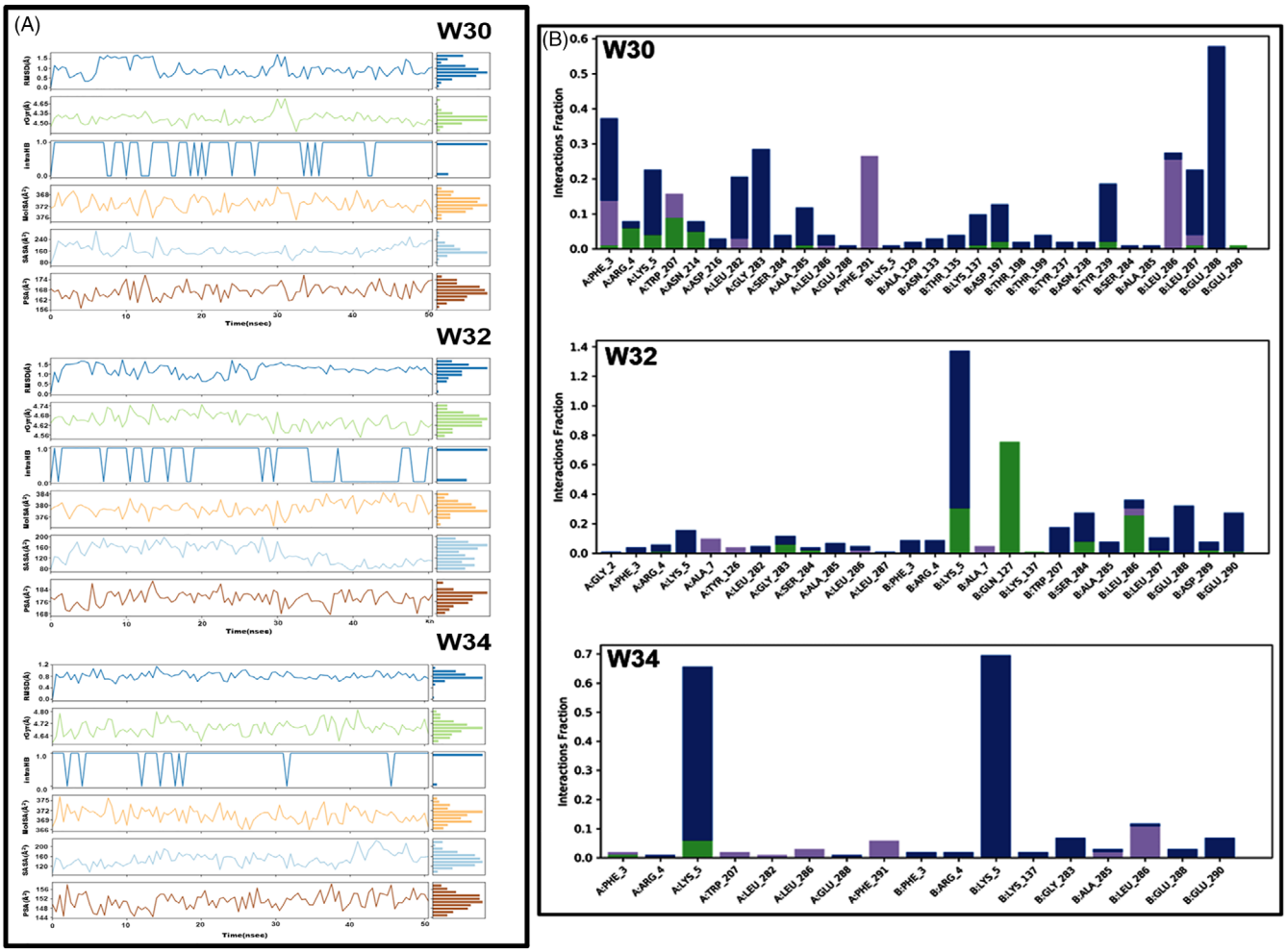

FIGURE 5 (A) Various measures of molecular dynamic simulations of top three compounds. Root mean square deviation (RMSD), radius of gyration (rGyr), intramolecular hydrogen bonds (intraHB), molecular surface area (MolSA), solvent accessible surface area (SASA), polar surface area (PSA). (B) Various intramolecular interactions made by top three compounds with M^{pro}, during molecular dynamics simulation. Color's code: Hydrogen bond (green), hydrophobic contacts (purple) and water-bridge (blue), withacoagulin H (W30), ajugin E (W32), and withacoagulin (W34)

TABLE 5 Computed ΔG (binding free energy change) of top three compounds against Mpro through MM/GBSA approach

S. no.	Compound name	MM/GBSA (KJ/mol)
1	Withacoagulin H (W30)	−63.463
2	Ajugin E (W32)	−56.140
3	Withacoagulin (W34)	−44.496

help reduce various other complications and inhibit viral replication.[11]

3.5 | Molecular dynamics and simulation

MD simulation study of 50 ns time scale of top three docked complexes (W30, W32, and W34) conducted to check for the stability in the active site of main protease of SARS-CoV-2. Although the top nine compounds may be potential candidates for *in-vitro* analysis, only these three were chosen for MD simulation because they formed a His-Cys dyad. Results were analyzed on various parameters generated by MD simulation, such as RMSD, RMSF, and interaction studies.

The stability of the simulation system and protein backbone conformational perturbations due to simulation were measured using the RMSD value.[34] From the RMSD graph, we predict that the protein backbone of the main protease was stable during the entire simulation time with a mean value of 2 Å. These lower fluctuations indicate the stable behavior of the protein backbone during the simulation. Comparing the docked complex RMSD trajectories, we inferred that W30 and W34 manifested fluctuations initially up to the 20 ns time scale. After 20 ns, the compound withacoagulin H did not reveal any significant RMSD fluctuations compared to the other compounds docked complex trajectories. The W30 docked complex trajectory was comparatively more stable with a mean value of 3 Å as compared to the other two compound trajectories. Moreover, the W30 trajectory is stable throughout the simulation, and changes in backbone were within the specified limits of RMSD (Figure 4(A)).

Further, RMSF analysis was performed to understand the docked complexes' residue-wise fluctuation. RMSF behavior was generated using the docked complexes; a plot was made using the RMSF, B factor, and interactions (Figure 4(B)). Peaks indicate most protein fluctuations; it is understood that N- and C-terminal fluctuate more than any other part of the protein. Also, the secondary structure elements revealed that alpha helices and beta strands are rigid compared to the loops more fluctuated (Figure S2).

Different parameters were calculated for the ligand to get insights into the conformational strain the ligand undergoes to maintain the protein-bound complex. The RMSD plot of W30 shows peaks of around ~1.5 Å. The rGyr measured for extendedness of the ligand, equivalent to its moment of inertia, was almost similar for all three ligands. The numbers of internal hydrogen molecules with ligand were more in the case of W30 shown by intramolecular surface area (intraHB) than other ligands. The molecular surface area (MolSA) was around 368–376 Å in W30. The solvent-accessible surface area (SASA) and polar surface area were ranging from 120 to 240 Å (Figure 5(A)). Further, the protein-ligand interactions were also assessed in the form of H-bonds, water-bridges, Ionic interactions, hydrophobic interactions, and so forth, to check the stability of the docked complexes. Figure 5(B) plots these different intermolecular interactions made by each pocket residue with its bound ligand.

3.6 | Binding free energy calculations

The free energy of binding of W30, W32, and W34 with M^{pro} of SARS-CoV-2 was computed using MM/GBSA approach. The free energy calculations are widely used and commonly accepted to estimate the ligand-binding affinities in the protein system. The ΔG (MM/GBSA) free energy calculated was −63.463 KJ/mol for W30, −56.140 KJ/mol for W32, and −44.496 KJ/mol for W34. All the binding energy values were negative, indicating that all the compounds' hits with protein were favorable. These results showed that W30 possesses maximum negative energy (−63.463 KJ/mol) than other compounds (Table 5). Therefore, it can be stated that withacoagulin H with minimum binding energy and better binding affinity could prove to be a better inhibitor for M^{pro} of SARS-CoV-2.

W30 becomes the compound of choice among all the screened compounds as it possesses an excellent binding affinity compared to other compounds. Interaction pattern shows its interaction with Hys41-Cys145 dyad, in simulation studies also its interaction with substrate binding region was maintained. In RMSD analysis, the fluctuations were within the acceptable range, making it a probable candidate. Further, W30 showed the least binding energy on MM/GBSA analysis than W32 and W34. Hence, it becomes probable compound obtained from *Withania* to act as a likely inhibitor for the M^{pro} of SARS-CoV-2.

4 | CONCLUSION

In conclusion, 73 withanolides and selected reference compounds were screened based on Lipinski's rule of five. The binding affinity of these screened compounds in the active sites of M^{pro} of SARS-CoV-2 was investigated further. Of these, nine molecules showed a significant docking score, even better than the reference compounds. ADME studies were also conducted for screened molecules to determine their drug-likeness and bioavailability. Since the molecules utilized here ADME was also determined, they can be the active lead for drug development of respective illness. The bioactive molecule from *Withania* showed good conformations with the M^{pro} of SARS-CoV-2, stable complex was formed; these complexes showed a more significant number of hydrogen bonds and van der Waals interactions than the complexes with reference compounds. Further, MD simulation studies confirm the stability of the compound W30 in the trajectory of the protein M^{pro} of SARS-CoV-2. MM/GBSA showed the least binding energy (−63.463 KJ/mol) for W30. Some more confirmatory analysis (both *in-vitro* and *in-vivo)* should be conducted for the screened molecules to ascertain their efficacy in the illness treatment.

CONFLICT OF INTEREST

The authors declare that they have no conflict of interest that could influence the work reported in this article.

ORCID

Muktesh Chandra https://orcid.org/0000-0002-6154-0647

REFERENCES

[1] N. Zhu, D. Zhang, W. Wang, X. Li, B. Yang, J. Song, X. Zhao, B. Huang, W. Shi, R. Lu, P. Niu, F. Zhan, X. Ma, D. Wang, W. Xu, G. Wu, G. F. Gao, W. Tan, *N. Engl. J. Med.* **2020**, *382*, 727. https://doi.org/10.1056/NEJMoa2001017

[2] N. Chen, M. Zhou, X. Dong, J. Qu, F. Gong, Y. Han, Y. Qiu, J. Wang, Y. Liu, Y. Wei, J. Xia, T. Yu, X. Zhang, L. Zhang, *Lancet* **2020**, *395*, 507. https://doi.org/10.1016/S0140-6736(20)30211-7

[3] L. Zhang, D. Lin, X. Sun, U. Curth, C. Drosten, L. Sauerhering, S. Becker, K. Rox, R. Hilgenfeld, *Science* **2020**, *368*, 409. https://doi.org/10.1126/science.abb3405

[4] P. C. Y. Woo, Y. Huang, S. K. P. Lau, K.-Y. Yuen, *Viruses* **2010**, *2*, 1804. https://doi.org/10.3390/v2081803

[5] C. Wu, Y. Liu, Y. Yang, P. Zhang, W. Zhong, Y. Wang, Q. Wang, Y. Xu, M. Li, X. Li, M. Zheng, L. Chen, H. Li, *Acta Pharm. Sin. B* **2020**, *10*, 766. https://doi.org/10.1016/j.apsb.2020.02.008

[6] Z. Jin, X. Du, Y. Xu, Y. Deng, M. Liu, Y. Zhao, B. Zhang, X. Li, L. Zhang, C. Peng, Y. Duan, J. Yu, L. Wang, K. Yang, F. Liu, R. Jiang, X. Yang, T. You, X. Liu, X. Yang, F. Bai, H. Liu, X. Liu, L. W. Guddat, W. Xu, G. Xiao, C. Qin, Z. Shi, H. Jiang, Z. Rao, H. Yang, *Nature* **2020**, *582*, 289. https://doi.org/10.1038/s41586-020-2223-y

[7] T. Pillaiyar, M. Manickam, V. Namasivayam, Y. Hayashi, S. H. Jung, *J. Med. Chem* **2016**, *59*, 6595. https://doi.org/10.1021/acs.jmedchem.5b01461

[8] N. J. Barrows, R. K. Campos, S. T. Powell, K. R. Prasanth, G. Schott-Lerner, R. Soto-Acosta, G. Galarza-Muñoz, E. L. McGrath, R. Urrabaz-Garza, J. Gao, P. Wu, R. Menon, G. Saade, I. Fernandez-Salas, S. L. Rossi, N. Vasilakis, A. Routh, S. S. Bradrick, M. A. Garcia-Blanco, *Cell Host Microbe* **2016**, *20*, 259. https://doi.org/10.1016/j.chom.2016.07.004

[9] S. He, B. Lin, V. Chu, Z. Hu, X. Hu, J. Xiao, A. Q. Wang, C. J. Schweitzer, Q. Li, M. Imamura, N. Hiraga, N. Southall, M. Ferrer, W. Zheng, K. Chayama, J. J. Marugan, T. J. Liang, *Sci. Transl. Med.* **2015**, *7*, 282ra49. https://doi.org/10.1126/scitranslmed.3010286

[10] Y. Kumar, H. Singh, C. N. Patel, *J. Infect. Public Health* **2020**, *13*, 1210. https://doi.org/10.1016/j.jiph.2020.06.016

[11] S. Verma, D. Twilley, T. Esmear, C. B. Oosthuizen, A.-M. Reid, M. Nel, N. Lall, *Front. Pharmacol.* **2020**, *11*. https://doi.org/10.3389/fphar.2020.561334

[12] Z. Wang, L. Yang, *Front. Pharmacol.* **2020**, *11*. https://doi.org/10.3389/fphar.2020.01013
[13] W. Vuong, M. B. Khan, C. Fischer, E. Arutyunova, T. Lamer, J. Shields, H. A. Saffran, R. T. McKay, M. J. van Belkum, M. A. Joyce, H. S. Young, D. L. Tyrrell, J. C. Vederas, M. J. Lemieux, *Nat. Commun.* **2020**, *11*. https://doi.org/10.1038/s41467-020-18096-2
[14] S. Maurya, M. Chandra, R. K. Yadav, L. K. Narnoliya, R. S. Sangwan, S. Bansal, P. Sandhu, U. Singh, D. Kumar, N. S. Sangwan, *Protoplasma* **2019**, *256*, 893. https://doi.org/10.1007/s00709-018-01338-y
[15] S. S. Ghoke, R. Sood, N. Kumar, A. K. Pateriya, S. Bhatia, A. Mishra, R. Dixit, V. K. Singh, D. N. Desai, D. D. Kulkarni, U. Dimri, V. P. Singh, *BMC Complement. Altern. Med.* **2018**, *18*. https://doi.org/10.1186/s12906-018-2238-1
[16] M. Chandra, S. Kushwaha, N. S. Sangwan, *Mol. Biol. Rep.* **2020**, *47*, 6587. https://doi.org/10.1007/s11033-020-05710-1
[17] V. K. Bhardwaj, R. Singh, J. Sharma, V. Rajendran, R. Purohit, S. Kumar, *J. Biomol. Struct. Dyn.* **2020**, *39*, 3449. https://doi.org/10.1080/07391102.2020.1766572
[18] R. V. Chikhale, S. K. Sinha, R. B. Patil, S. K. Prasad, A. Shakya, N. Gurav, R. Prasad, S. R. Dhaswadikar, M. Wanjari, S. S. Gurav, *J. Biomol. Struct. Dyn.* **2020**, 1. https://doi.org/10.1080/07391102.2020.1784289
[19] S. K. Sinha, S. K. Prasad, M. A. Islam, S. S. Gurav, R. B. Patil, N. A. AlFaris, T. S. Aldayel, N. M. AlKehayez, S. M. Wabaidur, A. Shakya, *J. Biomol. Struct. Dyn.* **2020**, 1. https://doi.org/10.1080/07391102.2020.1779132
[20] S. Verma, N. Lall, D. Meyer, *Evidence Based Validation of Traditional Medicines*, Vol. 873-900, Springer Singapore, Singapore **2021**.
[21] N. M. O'Boyle, M. Banck, C. A. James, C. Morley, T. Vandermeersch, G. R. Hutchison, *Aust. J. Chem.* **2011**, *3*. https://doi.org/10.1186/1758-2946-3-33
[22] G. M. Morris, R. Huey, W. Lindstorm, M. F. Sanner, R. K. Belew, D. S. Goodsell, A. J. Olson, *J. Comput. Chem.* **2009**, *30*, 2785. https://doi.org/10.1002/jcc.21256
[23] C. A. Lipinski, F. Lombardo, B. W. Dominy, P. J. Feeney, *Adv. Drug Delivery Rev.* **1997**, *23*, 3. https://doi.org/10.1016/S0169-409X(96)00423-1
[24] A. Daina, O. Michielin, V. Zoete, *Sci. Rep.* **2017**, *7*. https://doi.org/10.1038/srep42717
[25] K. J. Bowers, D. E. Chow, H. Xu, R. O. Dror, M. P. Eastwood, B. A. Gregersen, J. L. Klepeis, I. Kolossvary, M. A. Moraes, F. D. Sacerdoti, J. K. Salmon, Y. Shan, D. E. Shaw, SC '06: Proceedings of the 2006 ACM/IEEE Conference on Supercomputing; 20062006.
[26] T. Hou, J. Wang, Y. Li, W. Wang, *J. Chem. Inf. Model.* **2011**, *51*, 69. https://doi.org/10.1021/ci100275a.
[27] G. Schneider, *Nat. Rev. Drug Discov.* **2010**, *9*, 273. https://doi.org/10.1038/nrd3139
[28] H. Yang, M. Yang, Y. Ding, Y. Liu, Z. Lou, Z. Zhou, L. Sun, L. Mo, S. Ye, H. Pang, G. F. Gao, K. Anand, M. Bartlam, R. Hilgenfeld, Z. Rao, *Proc. Natl. Acad. Sci. U. S. A.* **2003**, *100*, 13190. https://doi.org/10.1073/pnas.1835675100
[29] O. Trott, A. J. Olson, *J. Comput. Chem* **2009**. https://doi.org/10.1002/jcc.21334
[30] N. Muralidharan, R. Sakthivel, D. Velmurugan, M. M. Gromiha, *J. Biomol. Struct. Dyn.* **2020**, *39*, 2673. https://doi.org/10.1080/07391102.2020.1752802
[31] C. Yung-Chi, W. H. Prusoff, *Biochem. Pharmacol.* **1973**, *22*, 3099. https://doi.org/10.1016/0006-2952(73)90196-2
[32] T. Steiner, *Angew. Chem. Int. Ed.* **2002**. https://doi.org/10.1002/1521-3773(20020104)41:1<48::AID-ANIE48>3.0.CO;2-U
[33] C. Y. Jia, J. Y. Li, G. F. Hao, G. F. Yang, *Drug Discovery Today* **2020**, *25*, 248. https://doi.org/10.1016/j.drudis.2019.10.014
[34] K. Sargsyan, C. Grauffel, C. Lim, *J. Chem. Theory Comput.* **2017**, *13*, 1518. https://doi.org/10.1021/acs.jctc.7b00028
[35] M. R. McGann, H. R. Almond, A. Nicholls, J. A. Grant, F. K. *Brown, Biopolymers: Original Research on Biomolecules*, **2003**, *68*, 76. https://doi.org/10.1002/bip.10207.

SUPPORTING INFORMATION

Additional supporting information may be found online in the Supporting Information section at the end of this article.

How to cite this article: S. Verma, C. N. Patel, M. Chandra, *J Comput Chem* **2021**, *42*(26), 1861. https://doi.org/10.1002/jcc.26717